

Gold nanoparticles functionalised with stable, fast water exchanging Gd^{3+} chelates as high relaxivity Contrast Agents for MRI

Miguel F. Ferreira^a, Bibimaryam Mousavi^b, Paula M. Ferreira^a, Catarina Martins,^c Lothar Helm^{*b}, José A. Martins^{*a}, Carlos F.G.C. Geraldes^c

^aCentro de Química, Campus de Gualtar, Universidade do Minho, 4710-057 Braga, Portugal. E-mail: jmartins@quimica.uminho.pt; Fax: +351253604382; Tel: +351253604385

^bLaboratoire de Chimie Inorganique et Bioinorganique, Ecole Polytechnique Fédérale de Lausanne, EPFL-BCH CH-1015 Lausanne, Switzerland. Email: lothar.helm@epfl.ch; Fax: +41 (0)21 693 98 95; Tel: +41 (0)21 693 98 76

^cDepartment of Life Sciences, Faculty of Science and Technology, and Center of Neurosciences and Cell Biology, University of Coimbra, P.O. Box 3046, 3001-401 Coimbra, Portugal. E-mail: geraldes@ci.uc.pt; Fax: +351239853607; Tel: +351239853608

Abstract: Gold nanoparticles functionalized with Gd^{3+} chelates displaying fast water exchange, superb pH stability and inertness towards transmetalation with Zn^{2+} have been prepared and characterized as a new high relaxivity (29 $mM^{-1}s^{-1}$, 30 MHz, 25 °C) Contrast Agent potentially safe for in vivo MRI applications. The Lipari-Szabo treatment for internal rotation was used to evaluate the effect of linker flexibility on the relaxivity of the gold nanoparticles. The relaxivity is limited by chelate flexibility. The effect of fast water exchange on the relaxivity of gold nanoparticles functionalized with Gd^{3+} chelates is also addressed in this communication.

Magnetic Resonance Imaging (MRI) is at the forefront of biomedical and clinical imaging. Its superb spatial resolution, non invasive nature and use of benign radiation outweigh its intrinsic low detection sensitivity. Paramagnetic relaxers can enhance dramatically the contrast between healthy and diseased tissues (Contrast Agents, CA's) by shortening the relaxation times of the water protons in their vicinity. The selective reduction of the relaxation times of the water protons brought about by a 1 mM concentration of paramagnetic centers, relaxivity (units $mM^{-1}.s^{-1}$), measures the efficacy of CAs.^{1,2} Gd^{3+} chelates are the most efficacious CAs for MRI. The Solomon-Bloembergen-Morgan (SBM) theory has established the physical-chemical principles guiding the design and synthesis of a plethora of CAs:³ multimeric, self-assembling, targeted, responsive, etc. Nonetheless, the predicted high relaxivities, of the order of magnitude $100 mM^{-1}s^{-1}$, are still to be achieved.

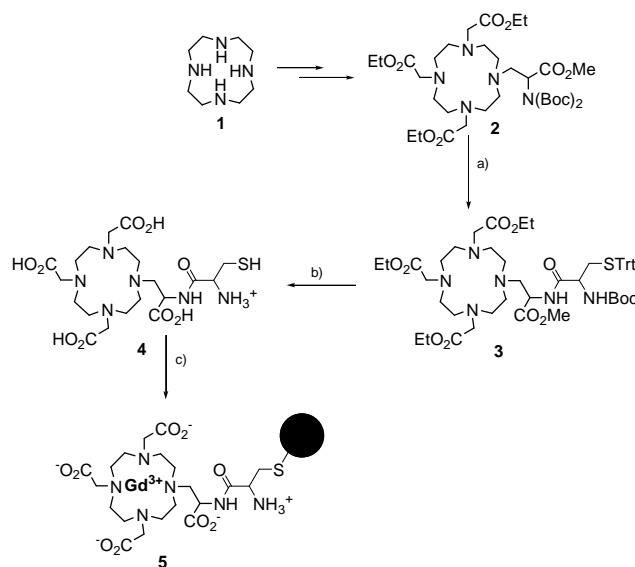
Nanotechnology is a promising new paradigm in Science and in biomedicine in particular. Different nanoplatfoms (nanoparticles, quantum dots, fullerenes, carbon nanotubes, viral capsules) have been used to improve the performance of CAs by integrating (intrinsic) reporting capabilities with properties inherent to nanosize and its interplay with biological systems and barriers.⁴

There is extensive accumulated experience on the use of Au compounds and colloidal (metallic) Au in medicinal chemistry. The accepted biocompatibility of gold allied to its resistance to oxidation and facile preparation of nanostructures displaying tunable size, shape (nanoparticles, nanorods) and surface properties, makes Au-NPs ideal objects for developing multifunctional CAs.⁵

Clustering of reporters on the surface of gold NPs (multimerisation) can lead to dramatic enhancements of detection sensitivity. Mixed monolayer nanoparticles containing reporters and targeting moieties allow integrating multimodality, targeting, imaging, and therapy (*e.g.* hyperthermia) in the same platform- theragnostics.

Au NPs functionalized with Gd³⁺ chelates are promising high relaxivity CAs for MRI.⁶ Spectacular relaxivities per nanoparticle (high density of relaxivity) have been attained by chelate clustering (multimerisation). Still, relaxivity enhancement per Gd³⁺ chelate is, in most cases, only moderate.^{7,8} This has been ascribed to suboptimal τ_R resulting from inefficient coupling of global (whole particle) and (independent) local rotational motions due to linker flexibility. Large surface curvature (small nanoparticles) and/or geometric constraints related to ligand structure prevent efficient monolayer packing, which would otherwise restrict linker/spacer flexibility.^{9,10} Helm and co-workers have reported so far, the most impressive relaxivity per Gd³⁺ chelate immobilized on gold nanoparticles, 60 mM⁻¹.s⁻¹ (30 MHz, 25 °C), using Gd³⁺ chelates of DTTA-type ligands.¹¹ Such high relaxivities have been ascribed to 2 exchanging inner sphere water molecules coupled to (complete) chelate rigidity. Relaxivity was limited by slow water exchange. In fact, most systems reported to date use Gd³⁺ chelates based on, facile to synthesize, DTPA-(*bis*)amide^{6,7,8} and DOTA-monoamide¹² ω -thiol ligands. Besides compromising the thermodynamic and kinetic stability of the chelates, critical for *in vivo* applications,¹³ amides display slow water exchange, in relation to their parent carboxylate chelates,¹⁴ limiting the relaxivity potentially achievable by rigid slow tumbling nanoparticles.¹¹ As far as we know, the effect of water exchange on the relaxivity of Au-NPs functionalized with Gd³⁺ chelates has not been explicitly addressed. We have reported recently the synthesis of a novel macrocyclic metal chelator of the DOTA-type- DO3A-*N*- α -aminopropionate. The Gd(DO3A-*N*- α -aminopropionate) chelate revealed exceptional inertness towards transmetallation, stability in a wide pH range (2-10) and fast water exchange, in the range considered ideal for attaining high relaxivities at intermediate fields.

The pendant amine group on the propionate arm can be used for conjugation purposes.¹⁵ Building on these results, we have demonstrated meanwhile that Gd³⁺ chelates of amide conjugates of the DO3A-*N*- α -aminopropionate chelator retain the fast water exchange and stability properties of its parent complex.^{15,16} A cysteine conjugate of the DO3A-*N*- α -aminopropionate ligand (**5**) (Scheme 1) was designed for decorating gold nanoparticles with Gd³⁺ chelates. Orthogonally protected prochelator **2** was synthesized in 3 steps from cyclen **1**¹⁵ (Scheme 1).



Scheme 1. Synthesis of cysteine conjugate DO3A-*N*-(α -cystamido)propionate (**4**) and preparation of gold nanoparticles functionalized with Gd(DO3A-*N*-(α -cystamido)propionate) chelates (**5**): a) i. TFA/DCM; ii. DIPEA/DCM, *N*-Boc-*S*-Trt-Cys, DCC/HOBt b) i. aqueous HCl, ii. Dowex1X2OH⁻ resin, elution with hydrochloric acid 0.1M; c) i. aqueous HAuCl₄, NaBH₄, ii) GdCl₃·6H₂O, iii) SEC- Sephadex G10, iv) dialysis- cellulose membrane MWCO 1000.

The amine group on compound **2** can be made available for conjugation by orthogonal deprotection with TFA. Conjugate **4** was prepared in reasonable yield, as a mixture of diastereoisomers, by coupling amine-deprotected bifunctional pro-chelator **2** with *N*-Boc-*S*-trityl cysteine using standard coupling conditions: DIPEA/DCC/HOBt. Purified amide was deprotected by sequential treatment with hydrochloric acid followed by Dowex1X2-OH⁻ resin and resin elution with diluted hydrochloric acid. Conjugate **4** was obtained as thiol, presumably due to the acidic conditions used for deprotection and resin elution. Gold nanoparticles functionalized with chelator **4** were prepared in aqueous medium using a modification of Brust's method.¹⁷ A molar equivalent of Gd³⁺, in relation to the amount of chelator used for nanoparticle preparation, was used to ensure complete loading of immobilized chelators.

A final purification step by Size Exclusion Chromatography (SEC) (Sephadex G10) followed by extensive dialysis (cellulose membrane MWCO 1.000) against water afforded the final nanoparticle preparation, free of soluble complex and Gd³⁺ ions. No attempt was made to fractionate the sample during SEC purification. The NPs are stable over extended time periods. They can be freeze-dried (and even rota-evaporated) and re-dissolved in water without any apparent aggregation and precipitation. Dynamic light scattering (DLS) analysis (Figure 3ASI) revealed nanoparticles displaying an average hydrodynamic diameter of about 3.9 nm. Transmission electron microscopy (TEM) analysis (Figure 4SI) confirmed this result showing spherical highly crystalline particles. The Au and Gd content of the NPs preparation were determined by inductively coupled plasma mass spectrometry (ICP-MS) analysis after digestion with *aqua regia* ([Au]= 3.77 mM; [Gd]= 1.24 mM; ratio Au/Gd=2.9). The thickness of the chelator monolayer on Au NPs displaying an hydrodynamic diameter (determined by DLS) of 4.8 nm has been estimated by molecular modeling as being around 1.3 nm.¹¹ Taking into consideration the structural differences between the chelates and linkers reported and the ones disclosed in this work, one could estimate the gold core diameter of our nanoparticles as around 1.9 nm. From these results, one can calculate that the Au core contains on average 210 Au atoms and the organic monolayer 70 Gd³⁺ chelates. A rough estimation gives that nearly all Au atoms at the surface are bonded to gadolinium chelates. The stability of the immobilized chelates regarding transmetallation against Zn²⁺, the most abundant endogenous metal ion, was evaluated by relaxometric measurements (25 °C, 20 MHz) using the protocol established for soluble Gd³⁺ chelates.¹⁸ The gold nanoparticles were challenged with phosphate buffer and phosphate buffer containing Zn²⁺ ions. The time evolution of the relaxivity (Figure 7BSI) suggests that virtually no transmetallation occurs over 30 hours. Moreover, the relaxivity is nearly constant in the pH range 2-12, indicating that immobilized chelates are stable (Figure 7ASI). Importantly, these assays evaluate also (whole) nanoparticle stability towards metal ion (Zn²⁺) and pH induced nanoparticle aggregation and precipitation, which would be apparent as time dependent relaxivity decrease. These results strongly suggest that the nanoparticles are safe for *in vivo* use, although further studies are necessary to evaluate chelate and nanoparticles stability in high protein media such as serum.

The nuclear magnetic relaxation dispersion (NMRD) profile was measured in the *Larmor* frequency range 0.01-400 MHz and fitted to the Solomon-Bloembergen-Morgan (SBM) theory including Lipari-Szabo treatment for internal rotation (Figure 1).¹⁹

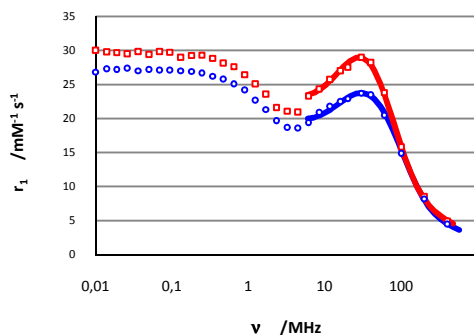


Figure 1. ¹H nuclear magnetic relaxation dispersion profiles for gold nanoparticles functionalized with Gd(DO3A-*N*-(α -cystamido)propionate) complex (5 mM): 25 °C (\square), and 37°C (\circ).

It was not possible to fit the whole NMRD profile, only frequencies above 6 MHz were fitted, as the SBM theory does not work properly at low magnetic fields for slow rotating objects. The best fit parameters obtained for the Au NPs from the analysis of ¹H NMRD data are shown in Table 1.

Table1. Best fit parameters obtained for Au NPs functionalized with Gd(DO3A-*N*-(α -cystamido)propionate) chelates from the fitting of the ¹H NMRD data.^{a,b}

Parameters	Value
$q(\text{H}_2\text{O})$	<u>$\frac{1}{2}$</u>
ΔH^\ddagger [J/mol]	<u>17</u> ^c
k_{ex}^{298} [10^7 s^{-1}]	<u>5.14</u> ^c
E_{R} [kJ/mol] (global)	18 ± 1.3
τ_{RH}^{298} [ps] (global)	2470 ± 151
E_{R} [kJ/mol] (local)	<u>18</u>
τ_{RH}^{298} [ps] (local)	177 ± 27
S^2	0.48 ± 0.02
E_{V} [kJ/mol]	<u>$\frac{1}{2}$</u>
τ_{V}^{298} [ps]	11 ± 1
Δ^2 [10^{20} s^{-2}]	0.040 ± 0.003

^aParameters underlined have been fixed; ^ba full list of parameters is given in Table 1SI; ^cref. 16

The water exchange rate constant and the activation enthalpy for water exchange were fixed in the fittings to values ($k_{ex}^{298} = 5.14 \times 10^7 \text{ s}^{-1}$ and $\Delta H^\ddagger = 17 \text{ J/mol}$) determined by us for the analogous low molecular weight chelate Gd(DO3A-*N*-(α -benzoylamido)propionate).¹⁶ As far as we are aware, there are no reports in the literature on the measurement of the exchange rate on Gd³⁺ chelates immobilized on gold nanoparticles. Several authors have reported independently that k_{ex} for the CA MS-325 drops by a factor of 2-3 upon binding to HSA.²⁰ Non-covalent (non-specific) association of Gd³⁺ chelates to hydrophobic pockets on large proteins (HSA) is bound to restrict water access to chelates. In the case of Au NPs, gadolinium chelates are covalently bound, in a well defined orientation, to the nanoparticles surface via a relatively long linker, ensuring unrestricted water access to chelates. It is thus reasonable to assume that the immobilization has no effect on the water exchange rate. Other parameters were fixed to values characteristic of DOTA-type chelates. The NMRD profile is characteristic of slow-rotating particles with a shallow decrease of r_1 at about 1 MHz and a broad peak centered at 20-30 MHz.^{11,21} Exceptional relaxivities per Gd³⁺ chelate (29 mM⁻¹s⁻¹, 30 MHz, 25 °C) were obtained comparing to other $q=1$ systems reported before.^{6-10,12} The temperature dependence of relaxivity at high field reveals that r_1 is not limited by water exchange. In fact, k_{ex}^{298} can be varied a lot in simulations without influencing the results. Chelate flexibility seems to be the main factor limiting relaxivity. In fact, the “modified Florence method”,²² which assumes (total) chelate rigidity is not suitable for fitting the NMRD data. The Lipari-Szabo treatment for internal rotation used in the fitting reveals a long global (whole particle) rotational correlation time ($\tau_{RH}^{298}{}_{\text{global}} = 2470 \text{ ps}$) and a short local rotational correlation time ($\tau_{RH}^{298}{}_{\text{local}} = 177 \text{ ps}$). The order factor value ($S^2 = 0.48$) is of the same order of magnitude as those reported before for micellar systems, reflecting chelate flexibility.²¹ This is somehow surprising considering the short (cystein) linker used for chelate immobilization. However, the structure of the linker might limit monolayer packing density, which could otherwise restrict local movements.^{9,10} The (unprecedented) high relaxivity per Gd³⁺ attained at intermediate field (29mM⁻¹s⁻¹, 30 MHz, 25 °C) together with the inertness and stability of the chelates and whole nanoparticles suggest that this system is promising for biological applications. It is also worth noting that the relaxivity peak at intermediate field is very broad extending into the high field region.

Relaxivity values at 100 and 200 MHz (15 and $8 \text{ mM}^{-1}\cdot\text{s}^{-1}$, respectively, at 37°C) are still remarkable for biological applications as a high field CA.²³ The relaxivity displayed by the system described by Helm and co-workers is limited by slow water exchange (rigid system, $S^2=1$). For the system described here, at magnetic fields relevant for MRI the relaxivity is limited by the flexibility of the linker used to bind the chelate to the nanoparticle (Fig. 8SI). Metal ion mediated self-assembly of Gd^{3+} complexes into rigid metallostars,²⁴ placement of Gd^{3+} chelates on the barycenter of sugar constructs²⁵ and anchoring Gd^{3+} chelates functionalized with two alkyl chains into micelles^{26,27} have been successful strategies for coupling local and global motions. It is thus conceivable, that Gd^{3+} chelates of conjugates of the DO3A-*N*- α -aminopropionate chelator, bearing long thiol linkers able to self-assemble into dense packing, rigid monolayers on Au, might attain unprecedented high relaxivities. The relaxation enhancement generated at 37°C and 1.5 T (60 MHz) by our Au-NPs is about $1,400 \text{ mM}^{-1}\cdot\text{s}^{-1}$ and therefore a local 700 nM concentration of particles would still lead to a relaxation enhancement of 1 s^{-1} .

This work was financially supported by Fundação para a Ciência e Tecnologia, Portugal: project PTDC/QUI/70063/2006; grant SFRH/BD/63994/2008 to Miguel Ferreira; Rede Nacional de RMN (REDE/1517/RMN/2005) for the acquisition of the Varian VNMRs 600 NMR spectrometer in Coimbra and the Bruker Avance-3 400 Plus in Braga. B. Mousavi and L. Helm acknowledge financial support by the Swiss National Science Foundation. This work was carried out within the COST D38 Action of the EU.

References.

- 1- P. Caravan, J. J. Ellison, T. J. McMurry and R. B. Lauffer, *Chem. Rev.*, 1999, **99**, 2293.
- 2- The Chemistry of Contrast Agents in Medical Magnetic Resonance Imaging, ed. A. E. Merbach and E. Toth, Wiley, Chichester, 2001.
- 3- C. S. Bonnet, E. Toth, *C. R. Chimie*, 2010, **13**, 700.
- 4- J. P. M. Almeida, A. L. Chen, A. Foster, R. Drezek, *Nanomedicine*, 2011, **6**, 815.
- 5- P. F. Jiao, H. Y. Zho, L. X. Chen, B. Yan, *Current Med. Chem.*, 2011, **18**, 2086.
- 6- C. Alric, J. Taleb, G. Le Duc, C. Mandon, C. Billotey, A. Le Meur-Herland, T. Brochard, F. Vocanson, M. Janier, P. Perriat, S. Roux, O. Tillement, *J. Am. Chem. Soc.*, 2008, **130**, 5908.
- 7- P.-J. Debouttiere, S. Roux, F. Vocanson, C. Billotey, O. Beuf, A. Favre-Reguillon, Y. Lin, S. Pellet-Rostaing, R. Lamartine, P. Perriat, O. Tillement, *Adv. Funct. Mater.* 2006, **16**, 2330.

- 8- J.-A. Park, P.A.N. Reddy, H.-K. Kim, L.-S. Kim, G.-C. Kim, Y. Chang, T.-J. Kim, *Bioorg. Med. Chem. Lett.* 2008, **18**, 6135.
- 9- M. F. Warsi, R. W. Adams, S. B. Duckett, V. Chechik, *Chem. Commun.*, 2010, **46**, 451.
- 10- M. F. Warsi, V. Chechik, *Phys. Chem. Chem. Phys.*, 2011, **13**, 9812.
- 11- L. Moriggi, C. Cannizzo, E. Dumas, C. R. Mayer, A. Ulianov, L. Helm, *J. Am. Chem. Soc.*, 2009, **131**, 10828.
- 12- M. Marradi, D. Alcantara, J. M. de la Fuente, M. L. García-Martín, S. Cerdán, S. Penadés, *Chem. Commun.*, 2009, 3922.
- 13- H. Pietscha, G. Jost, T. Frenzela, M. Raschkeb, J. Walterb, H. Schirmerc, J. Hüttera, M. A. Siebera, *European Journal of Radiology*, 2011, **80**, 349.
- 14- D. H. Powell, O. N. NiDhubhghaill, D. Pubanz, L. Helm, Y. S. Lebedev, W. Schlaepfer, A. E. Merbach, *J. Am. Chem. Soc.*, 1996, **118**, 9333.
- 15- M. F. Ferreira, A. F. Martins, J. A. Martins, P. M. Ferreira, E. Toth, C. F. G. C. Geraldes, *Chem. Commun.*, 2009, 6475.
- 16- M. F. Ferreira, A. F. Martins, C. I. O. Martins, E. Tóth, T. B. Rodrigues, D. Calle, S. Cerdan, P. López-Larrubia, J. A. Martins and C. F. G. C. Geraldes, Amide conjugates of the DO3A-*N*-(α -amino)propionate ligand: leads for stable, high relaxivity Contrast Agents for MRI?, manuscript submitted to Contrast Media and Molecular Imaging.
- 17- M. Brust, M. Walker, D. Bethell, D. J. Schiffrin, R. Whyman, *Chem. Commun.*, 1994, 801.
- 18- S. Laurent, L. V. Elst, C. Henoumont, and R. N. Muller, *Contrast Media Mol. Imaging*, 2010, **5**, 305.
- 19- F. A. Dunand, E. Toth, R. Hollister, A. E. Merbach, *J. Biol. Inorg. Chem.*, 2001, **6**, 247.
- 20- P. Caravan, N. J. Cloutier, M. T. Greenfield, S. A. McDermid, S. Dunham, J. W. M. Bulte, J. C. Amedio Jr., R. J. Looby, R. M. Supkowski, W. Horrocks Jr, T. J. McMurry, R. B. Lauffer, *J. Am. Chem. Soc.*, 2002, **124**, 3152.
- 21- S. Torres, J. A. Martins, J. P. André, C.F.G.C. Geraldes, A. E. Merbach, É. Tóth, *Chem. Eur. J.*, 2006, **12**, 940.
- 22- L. Bertini, O. Galas, C. Luchinat, G. Parigi, *J. Magn. Reson.*, 1995, **113A**, 151.
- 23- L. Helm, *Future Medicinal Chemistry*, 2010, **2**, 385.
- 24- J. B. Livramento, E. Toth, A. Sour, A. Borel, A. E. Merbach, R. Ruloff, *Angew. Chem. Int. Ed.* 2005, **44**, 1480.

- 25- D. A. Fulton, E. M. Elemento, S. Aime, L. Chaabane, M. Botta, D. Parker, *Chem. Commun.*, 2006, 1064.
- 26- F. Kielar, L. Tei, E. Terreno, M. Botta, *J. Am. Chem. Soc.*, 2010, **132**, 7836.
- 27- C. Vanasschen, N. Bouslimani, D. Thonon, J. F. Desreux, *J. Inorg. Chem.* 2011, **50**, 8946.

Supplementary information

Materials and methods

Chemicals were purchased from Sigma-Aldrich and used without further purification. Cyclen was purchased from Chematech, France. Analytical grade solvents were used and, unless specified, not further purified. Reactions were monitored by TLC on silica gel by examination under UV light (250 nm) and staining with iodine vapour. Preparative chromatography was carried on Silica Gel 60 (230-400 mesh). Ion exchange chromatography was performed on Dowex 1X2 OH⁻ (50-100 mesh) resin. Size Exclusion Chromatography (SEC) was performed on Sephadex G10 (40-120 μ m). Dialysis was performed against water on cellulose membranes with MWCO of 1kDa. UV-VIS spectra were acquired with a Shimadzu UV-2501PC spectrophotometer. The size distribution and zeta potential of the gold nanoparticles were determined with a Malvern Zetasizer, NANO ZS (Malvern Instruments Limited, UK), using a He-Ne laser (wavelength of 633 nm) and a detector angle of 173°. Mass spectrometry was performed at CACTI- Vigo, Spain. ¹H and ¹³C NMR spectra were run on Varian Unity Plus 300, Bruker Avance-3 400 Plus and Varian VNMRs 600 NMR spectrometers. Chemical shifts (δ) are given in ppm relative to the CDCl₃ solvent (¹H, δ 7.27; ¹³C 77.36) as internal standard. For ¹H and ¹³C NMR spectra recorded in D₂O, chemical shifts (δ) are given in ppm, respectively, relative to TSP as internal reference (¹H, δ 0.0) and *tert*-butanol as external reference (¹³C, CH₃ δ 30.29). ¹³C NMR spectra were proton broadband decoupled using a GARP-1 modulated decoupling scheme.

The ¹H Nuclear Magnetic Resonance Dispersion (NMRD) measurements were performed by using a Stellar Spinmaster FFC NMR relaxometer (0.01-20 MHz) equipped with a VTC90 temperature control unit. At higher fields, the ¹H relaxivity measurements were performed on Bruker Minispecs mq30 (30 MHz), mq40 (40 MHz) and mq60 (60 MHz), as well as Bruker Avance spectrometers connected to 2.35 T, 4.7 T and 9.4 T superconducting magnets. In each case, the temperature was measured by a substitution technique. Variable temperature measurements were performed at 25 and 37 °C. The relaxometric pH dependence and transmetallation studies with Zn²⁺ of the nanoparticles were performed on a Bruker Minispec mq20 (20 MHz). The NMRD profiles have been analysed using the Visualiseur/Optimiseur 3.6 program¹ running on a Matlab® 6.5 platform.

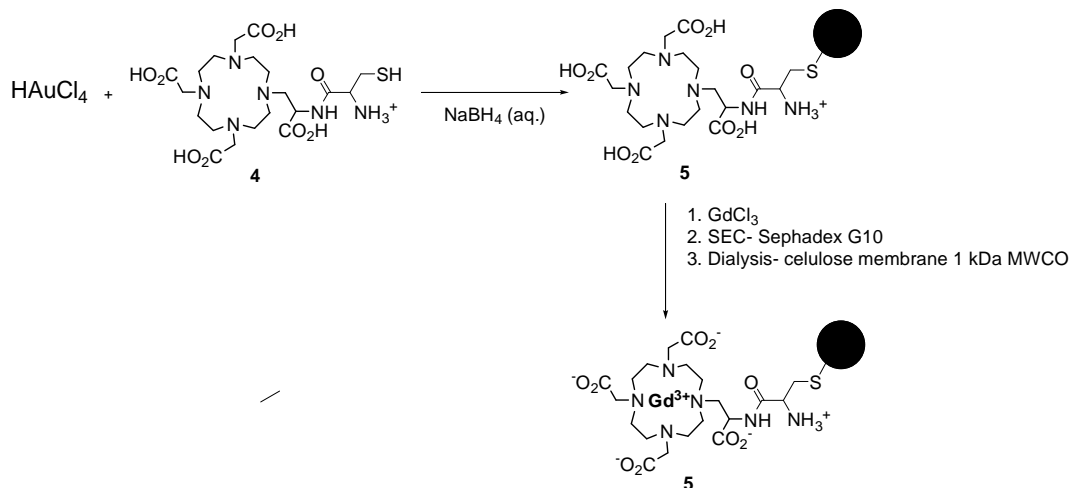
Synthesis and characterization

Preparation of the DO3A-*N*-(α -cystamido)propionate ligand (4):

Synthesis of amide (3): Orthogonally protected cyclen **2**² (1.62 g, 2.21 mmol) was dissolved in a mixture of dichloromethane/trifluoroacetic acid (45 cm³, 1/3 v/v) and stirred overnight at room temperature. The solvent was evaporated at reduced pressure and the residue was re-dissolved in dichloromethane and evaporated again. This procedure was repeated several times to give a thick light yellow oil. ¹H NMR spectroscopy (CDCl₃) revealed the disappearance of the signals assigned to the *Boc* groups in precursor compound **2**. The integration ratio between the methine proton NCH₂CH and the methyl or methylene protons (from the ethyl ester groups) indicated that no deprotection of the ethyl ester groups occurred. Amine deprotected compound (**2**) (2.21 mmol, assuming quantitative deprotection) was dissolved in dichloromethane (30 cm³). The solution was adjusted to pH 8-9 (pH paper) by dropwise addition of DIPEA (~7.0 cm³). To this solution was sequentially added *N*-Boc-*S*-trityl-*L*-cysteine (1.02 g, 2.21 mmol), Hydroxybenzotriazole (0.557 g, 2.64 mmol) and a solution of DCC (0.752 g, 2.64 mmol) in dichloromethane (5 cm³). The reaction mixture was left stirring at room temperature overnight. The DCU byproduct was removed by filtration and the sample was concentrated under reduced pressure. The residue was re-dissolved in ethyl acetate (100 cm³), and the solution was washed sequentially with KHSO₄ (1M, 3 x 30 cm³), NaHCO₃ (saturated solution, 3 x 30 cm³) and brine (3 x 30 cm³). The organic phase was concentrated under reduced pressure and the residue was purified by a flash chromatography (100% CH₂Cl₂ → CH₂Cl₂/EtOH (70:30)) to afford amide (**3**) (0.736 g, 34%). ¹H NMR (300 MHz, CDCl₃): δ = 1.26 (m, 9 H, C(O)OCH₂CH₃), 1.46 (s, 9H, C(CH₃)₃), 2.2-3.60 (broad, overlapped signals with a integration corresponding to 26 H; N(CH₂)₂N, NCH₂CO₂Et, NHBocCH_aH_bCH, NCH_aH_bCH), 3.80 (s, 3H, C(O)OCH₃), 4,15 (m, 6H, OCH₂CH₃), 4.77 (m (br), 1H, NHBocCH_aH_bCH), 5.87 (m (br), 1H, NCH_aH_bCH), 7.1-7.6 (m, 15 H, Trt). HRMS (ESI): m/z: calcd for C₅₁H₇₃N₆O₁₁S [M+H]⁺: 977.5058, found: 977.5021.

Preparation of fully deprotected DO3A-*N*-(α -cystamido)propionate metal chelator (4): Compound (3) (0.706 g, 0.722 mmol) was dissolved in hydrochloric acid 3 M (20 cm³; water (5 cm³)/ethanol (10 cm³)/hydrochloric acid 37% (5 cm³). The solution was left stirring at room temperature overnight. The solvent was removed under reduced pressure at room temperature and the residue was taken up into a small volume of water (~ 20 cm³) and filtered. The solution was concentrated at reduced pressure, the residue was dissolved in water (~ 15 cm³) and the solution was adjusted to pH ~ 10-11 by adding small portions of Dowex 1X2-100-OH⁻ resin. The suspension was kept under stirring at room temperature for 2 hours. The wet resin was transferred into a chromatography column, washed with water (~ 50 cm³) and eluted with 0.1 M hydrochloric acid. The relevant fractions, identified by TLC (ethanol water 1/1, revelation with iodine vapor) were pooled, concentrated at room temperature and further dried under vacuum to afford the final deprotected compound (4) in the hydrochloride form, as a light yellow solid (0.276 g, 71.2%). ¹H NMR (300 MHz, D₂O): δ = 2.2-4.40 (broad, overlapped signals with an integration corresponding to, 22 H: N(CH₂)₂N and NCH₂COOH), 3.07 (m, 2H, CH₂SH), 3.33 (m, 2H, CH₂CH), 4.22 (m, 1H, CH₂CH), 4.61 (m, 1H, SHCH₂CH). ¹³C NMR (75.4 MHz, D₂O): selected signals: 22.14 (CH₂SH), 46.34 (CH₂), 47.63 (CH₂), 48.16 (CH₂), 48.69 (CH₂), 49.98 (CH₂), 51.01 (CH₂), 53.43 (CH₂), 53.80 (CH₂CH), 54.03 (CHCH₂SH), 54.14 (CH₂), 54.27 (CH₂), 55.15 (CHCH₂), 56.09 (CH₂), 169.03 (NHC(O)), 169.14 (C(O)), 170.60 (C(O)), 176.61 (CHC(O)), 177.93 (C(O)). HRMS (ESI): m/z: calcd for C₂₀H₃₇N₆O₉S [M+H]⁺: 537.2343, found: 537.2325.

Preparation gold nanoparticles functionalized with Gd(DO3A-*N*-(α -cystamido) propionate) chelates: The strategy envisaged for preparing gold nanoparticles functionalized with Gd(DO3A-*N*-(α -cystamido)propionate) chelates is depicted (as cartoon) in Scheme 1SI).



Scheme 1SI. General strategy (cartoon representation) for the preparation of gold nanoparticles functionalized with Gd(DO3A-*N*-(α -cystamido)propionate) chelates.

An aqueous solution of DO3A-*N*-(α -cystamido)propionate (**4**) ligand (46.13 mM, 4.66 cm³, 0.099 mmol) was added dropwise, under magnetic stirring, to an aqueous solution of $\text{H[AuCl}_4\text{]}$ (58.85 mM, 1.64 cm³, 0.096 mmol; molar ratio Au/ligand (1/1)). Addition of the ligand to the Au^{3+} solution generated initially a dark orange color which faded away with further ligand addition. To the stirring reaction mixture was added, in one aliquot, a solution of NaBH_4 (20.40 mM, 0.217 cm³, 0.094 mmol; molar ratio Au/ligand/ NaBH_4 1/1/1). The reaction mixture turned immediately dark brown and was left stirring at room temperature for 24 hours. The nanoparticles preparation was adjusted to pH \sim 7.0 with aqueous NaOH 1 M and filtered through a 0.20 μm PTFE syringe filter. A small sample (1.0 cm³) was kept for further characterization. To the remaining sample (\sim 6.0 cm³) was added a solution of $\text{GdCl}_3 \cdot 6\text{H}_2\text{O}$ (0.0211 g, 0.080 mmol; 1 molar equivalent in relation to the total amount of ligand used in the nanoparticles synthesis) in water (1.0 cm³). During the addition of the Gd^{3+} ion the solution was kept at pH \sim 5.5 by adding NaOH 0.1 M. The reaction mixture was left stirring at room temperature for 24 hours, adjusted to pH \sim 7 by with aqueous NaOH (1 M solution) and filtered through a 0.20 μm PTFE syringe filter. The gold nanoparticle preparation was purified by size exclusion chromatography using Sephadex G10 (40-120 μm) eluting with water.

During elution a colored broad band separated in the column. No attempt was made to fractionate the sample, the full band was collected as a single fraction ($\sim 20 \text{ cm}^3$). The nanoparticles preparation was further purified by dialysis against water using a cellulose membrane with 1 KDa MWCO. The xylenol orange test indicated the absence of free Gd^{3+} in the gold nanoparticles preparation. The Gd and Au concentration of the nanoparticle's preparation ($[\text{Au}] = 3.77 \text{ mM}$; $[\text{Gd}] = 1.24 \text{ mM}$; $[\text{Au}]/[\text{Gd}] = 2.9$) was determined by ICP analysis.

The binding mode of the Gd(DO3A-*N*-(α -cystamido)propionate) chelates to the gold surface, represented in Scheme 1SI through the thiol group of the cysteine linker, is the most likely anchorage mode. Several authors have suggested the simultaneous binding of the thiol and amine groups of cysteine to gold (forming a chelate ring) as the (most likely) anchorage mode of cysteine containing peptides to gold NPs.³ The band at 3500 cm^{-1} in the IR spectrum (KBr pellets) of our nanoparticles (Figure 1SI) is assigned by several authors to vibrational modes of the $-\text{NH}_3^+$ group in cysteine functionalized gold nanoparticles.⁴

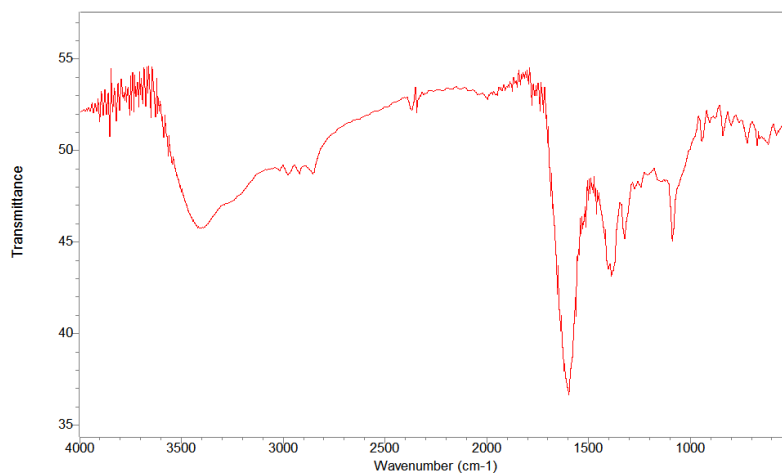


Figure 1SI. IR spectrum (KBr) of gold NPs functionalized with Gd(DO3A-*N*-(α -cystamido)propionate) chelates

The IR spectrum of the functionalized gold NPs suggests that the nanoparticles are linked to the gold core through the thiol group only. The broad band at around 3500 cm^{-1} has been assigned to vibrational modes of the $-\text{NH}_3^+$ in cysteine functionalized gold NP's.^{3,4} If the amine group is not involved in the binding to gold, then the effect of the solution pH on the overall charge of the immobilized complexes should be apparent as a pH-dependent zeta potential.

The negative Zeta potential values measured at pH 7.0 and 10.0 (Figure 3BSI) suggest that the chelates (and whole nanoparticles) bear net negative charges. Moreover, the value and shape of the Zeta potential distribution curves at pH 7.0 and 10.0 suggests a higher extent of ionization of the amine group at pH 10. None the less the putative ionization of the amine group seems not to affect substantially the relaxivity of the NP's in the pH range 2-12 (Figure 7ASI).

UV-VIS spectroscopy

A very ill-defined plasmon band is apparent in the UV-VIS spectrum of the gold nanoparticles functionalized with Gd(DO3A-*N*-(α -cystamido)propionate) chelates, suggesting that the nanoparticles display a diameter bellow 6 nm.

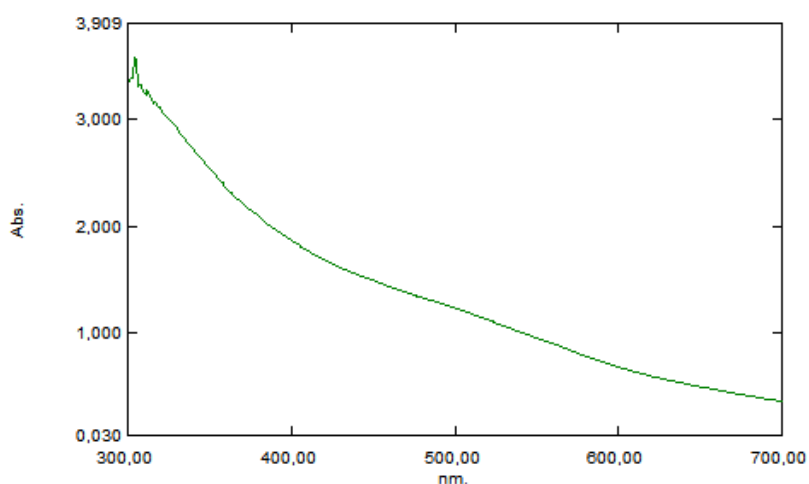
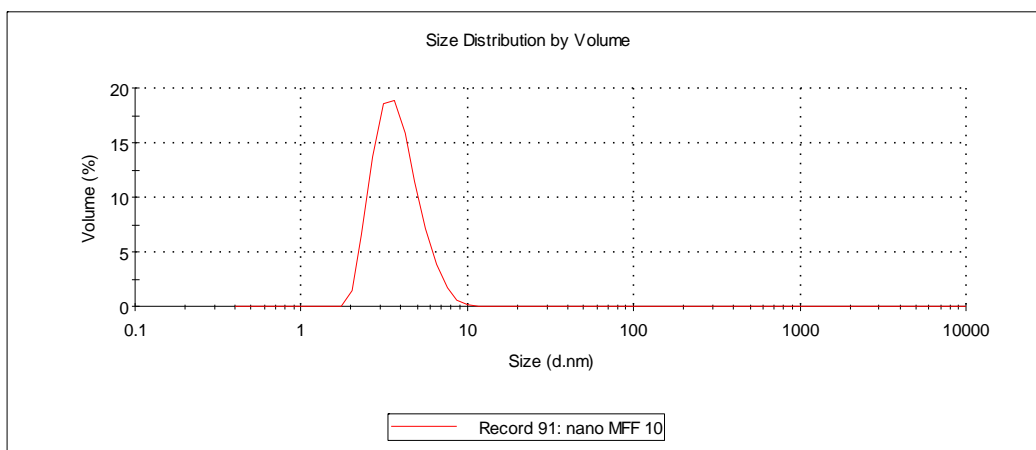


Figure 2SI. UV-VIS spectrum for the preparation of nanoparticles functionalized with Gd(DO3A-*N*-(α -cystamido)propionate) chelates (diluted by a factor of 3, pH 7.0).

Size and zeta potential characterization by DLS



Peak	Diam. (nm)	% Volume	Width (nm)
	3.885	100	1.258

Figure 3ASI. DLS size distribution (Volume) for the preparation of nanoparticles functionalized with Gd(DO3A-*N*-(α -cystamido)propionate) chelates at pH 7.0.

From the DLS experiments (Figure 3ASI), one can conclude that the main population of nanoparticles in solution displays an average hydrodynamic diameter around 3.9 nm.

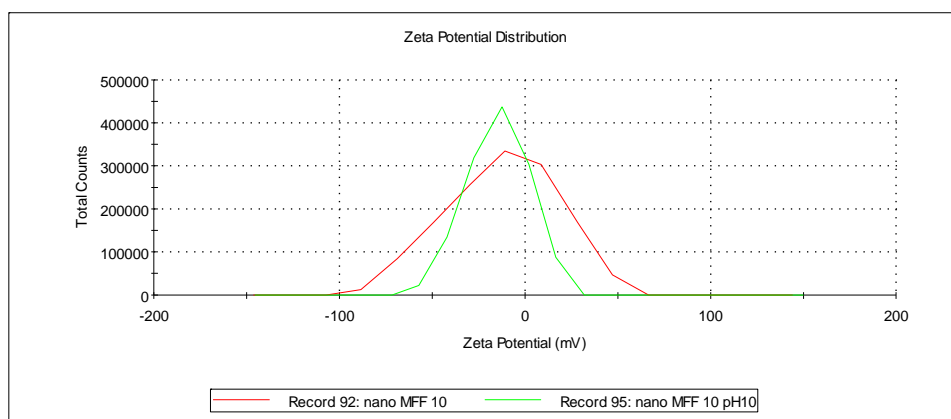


Figure 3BSI. Zeta potential distribution at pH 7.0 (red curve) and pH 10.0 (green curve) for the preparation of nanoparticles functionalized with Gd(DO3A-*N*-(α -cystamido)propionate) chelates.

Figure 3BSI shows that the nanoparticles display negative zeta potential both at pH 7.0 and pH 10.0, with a broader distribution at pH 7.0.

TEM characterization of the nanoparticles

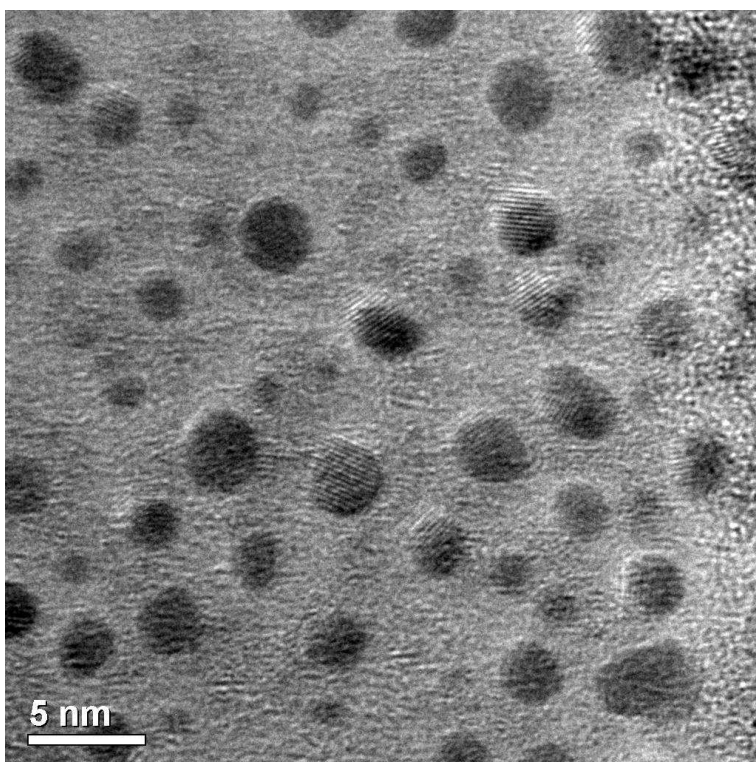
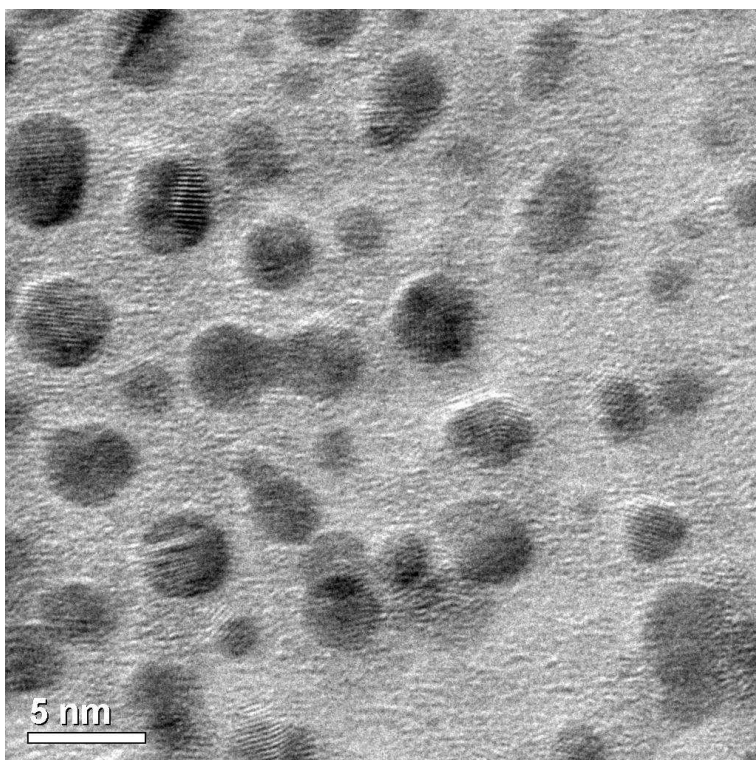


Figure 4SI. TEM images of the Au-NPs. The images were acquired with a JEOL 2010 UHR transmission electron microscope at the Interdisciplinary Centre for Electron Microscopy (CIME) at EPFL, Lausanne. TEM samples have been prepared by dropping solutions of gold nanoparticles onto carbon-coated-copper grids and evaporating the solvent (water) to dryness.

Estimation of the number of Au atoms

The diameter of the Au-core of the gold nanoparticles has been estimated by choosing the thickness of the organic layer at the surface as 1 nm. This layer should be less thicker than in ref. 6 because there are only 4 connecting atoms between the N in the chelate and the S at the Au surface compared to 5 in ref. 6. The Au-core has therefore a diameter of ~1.9 nm. Following ref. 7 the total number of Au atoms can be estimated to be ~210 from $N_{\text{Au}} = 30.9 \cdot D^3$. Taking the experimental Au/Gd ratio of 2.9 there are ~70 Gd^{3+} -ions bound to a particle which corresponds roughly to 1 Gd^{3+} ion per gold atom at the surface.

Relaxometric characterization of the gold nanoparticles

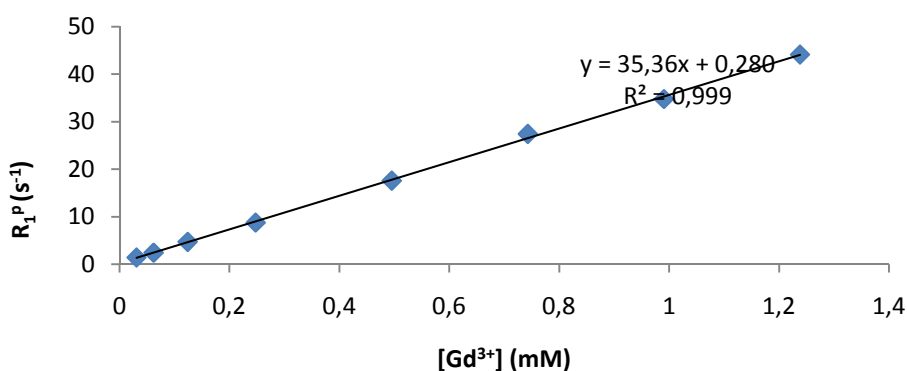


Figure 5SI. Dependence of the proton longitudinal paramagnetic relaxation rates (R_{1p}) on the Gd^{3+} concentration for the preparation of nanoparticles functionalized with $\text{Gd}(\text{DO3A}-N-(\alpha\text{-cystamido})\text{propionate})$ chelates (20 MHz, 25 °C, pH 7.5). Preparations with different concentrations Gd^{3+} were obtained by dilution of the stock solution [Gd^{3+}]= 1.238 mM.

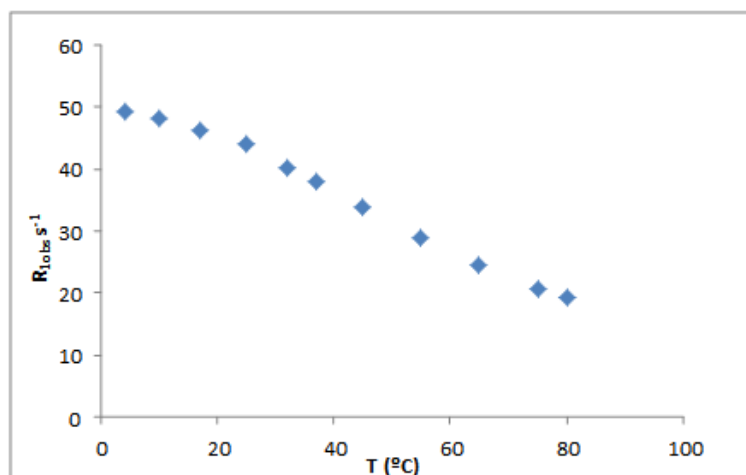


Figure 6SI. Dependence of the proton longitudinal paramagnetic relaxation rates (R_{1p}) on temperature for the preparation of nanoparticles functionalized with Gd(DO3A-*N*-(α -cystamido)propionate) chelates ($[Gd^{3+}] = 1.238$ mM, 20 MHz, 25 °C, pH 7.5).

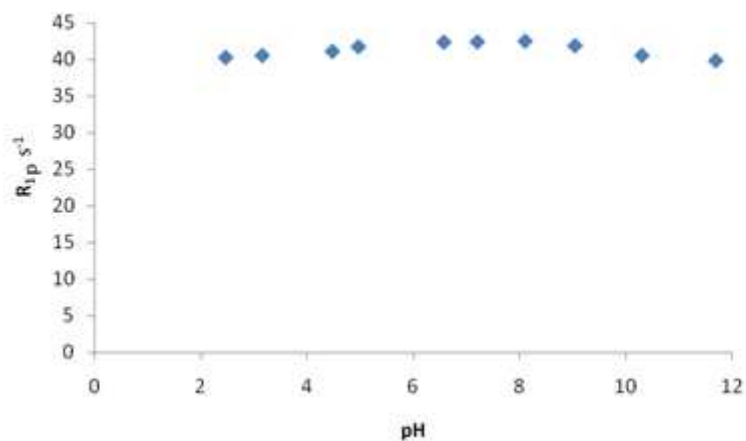


Figure 7ASI. Dependence of the proton longitudinal paramagnetic relaxation rates (R_{1p}) on the solution's pH for the preparation of nanoparticles functionalized with Gd(DO3A-*N*-(α -cystamido)propionate) chelates ($[Gd^{3+}] = 1.238$ mM, 20 MHz, 25 °C).

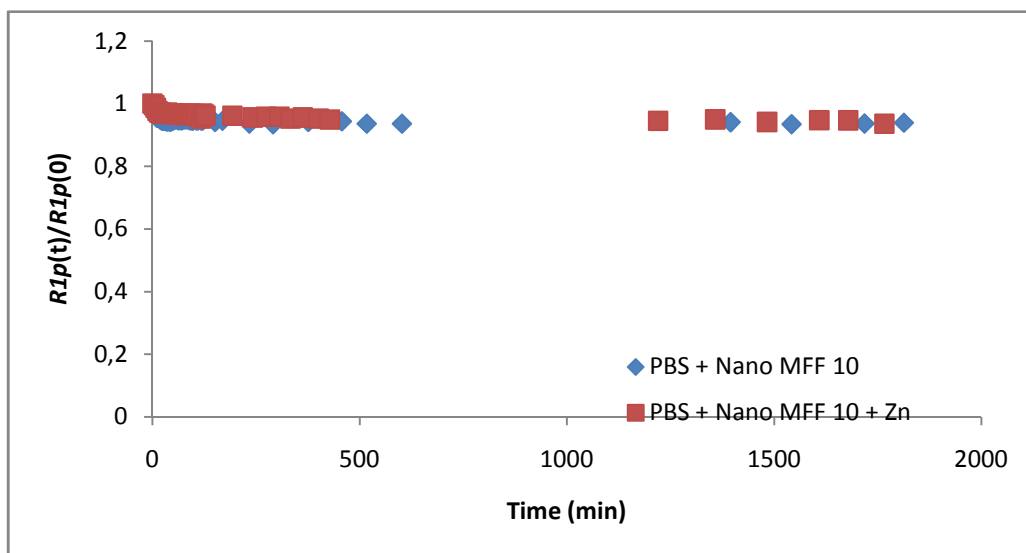


Figure 7BSI. Time evolution of the relative water proton paramagnetic relaxation rate $R_{1p}(t)/R_{1p}(0)$ (20 MHz, 37 °C) for the preparation of nanoparticles functionalized with Gd(DO3A-*N*-(α -cystamido)propionate) chelates ($[Gd^{3+}] = 0.928$ mM) in PBS 2.5 mM, pH 7.1 in the presence (●) and in the absence (◆) of 0.75 mM $ZnCl_2$.

Fitting of NMRD profiles

Table 1SI. Full list of parameters used for the fitting of the high-field part of the NMRD profiles using SBM theory.

Parameters	Value
$q(\text{H}_2\text{O})$	<u>1</u>
ΔH^\ddagger [J/mol]	<u>17^a</u>
k_{ex}^{298} [10^7 s^{-1}]	<u>5.14^a</u>
E_{R} [kJ/mol] (global)	18 ± 1.3
τ_{RH}^{298} [ps] (global)	2470 ± 151
E_{R} [kJ/mol] (local)	<u>18^b</u>
τ_{RH}^{298} [ps] (local)	177 ± 27
S^2	0.48 ± 0.02
E_{V} [kJ/mol]	1
τ_{V}^{298} [ps]	11 ± 1
Δ^2 [10^{20} s^{-2}]	0.040 ± 0.003
r_{GdH} [Å]	<u>3.1^c</u>
D_{GdH}^{298} [$10^{-10} \text{ m}^2 \text{ s}^{-1}$]	<u>23^c</u>
$E_{D\text{GdH}}^{298}$ [kJ/mol]	<u>20^c</u>
d [Å]	<u>3.6^c</u>

Parameters underlined have been fixed: ^a from reference 5; ^b fixed to $E_{\text{R}}(\text{global})$ after a preliminary fit, ^c fixed to usual parameters

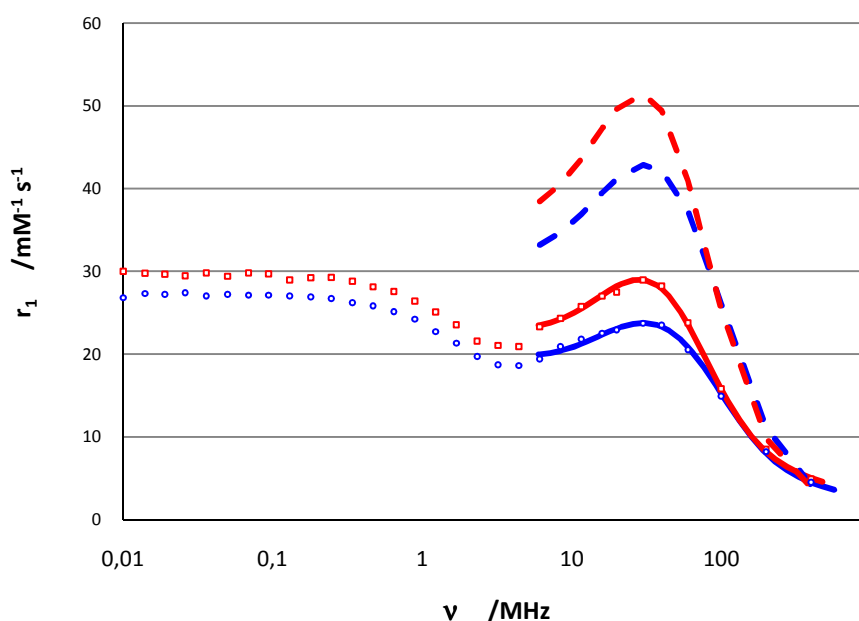


Figure 8SI. ^1H nuclear magnetic relaxation dispersion profiles for gold nanoparticles functionalized with Gd(DO3A-*N*-(α -cystamido)propionate) complex (5 mM): 25 °C (\square), and 37°C (\circ). The full drawn lines are from the fit with parameters in Table 1SI. The dashed lines are calculated using the same parameters except $S^2 = 1$.

References

1. F. Yerly, EPFL, Lausanne, edn, 2008.
2. M. F. Ferreira, A. F. Martins, J. A. Martins, P. M. Ferreira, E. Toth, C. F. G. C. Geraldes, *Chem. Commun.*, **2009**, 6475
3. R. Lévy, N. T. K. Thanh, R. C. Doty, I. Hussain, R. J. Nichols, D. J. Schiffrin, M. Brust, D. G. Fernig, *J. Am. Chem. Soc.*, **2004**, 126, 10077.
4. S. Aryal , B. K. C. Remant, N. Dharmaraj, N. Bhattarai , C. H. Kimc, H. Y. Kimc, *Spectrochimica Acta Part A*, 2006, **63**, 160.
5. M. F. Ferreira, A. F. Martins, C. I. O. Martins, E. Tóth, T. B. Rodrigues, D. Calle, S. Cerdan, P. López-Larrubia, J. A. Martins and C. F. G. C. Geraldes, Amide conjugates of the DO3A-*N*-(α -amino)propionate ligand: leads for stable, high relaxivity Contrast Agents for MRI?, manuscript submitted to Contrast Media and Molecular Imaging.
6. L. Moriggi, C. Cannizzo, E. Dumas, C. R. Mayer, A. Ulianov, L. Helm, *J. Am. Chem. Soc.*, 2009, **131**, 10828.
7. X. Liu, M. Atwater, Ji. Wang, Q. Huo, *Coll. Surf. B: Biointerfaces*, 2007, **58**, 3.